JQS

Journal of Quaternary Science



Southern Baffin Island mean annual precipitation isotopes modulated by summer and autumn moisture source changes during the past 5800 years

DEVON B. GORBEY,¹* DELIZABETH K. THOMAS,¹ DESARAH E. CRUMP,^{2,3} DELIZABETH K. THOMAS,¹ DESARAH E. CRUMP,^{2,3} DELIZABETH K. HOLLISTER,¹ DELIZABETH K. THOMAS,¹ D

Received 31 March 2021; 14 September 2021; Accepted 2 October 2021

ABSTRACT: Paleo water isotope records can elucidate how the Arctic water cycle responded to past climate changes. We analyze the hydrogen isotope composition (δ^2H) of plant-derived n-alkanoic acids (waxes) from Lake Qaupat, Baffin Island, Nunavut, Canada, to assess moisture sources and seasonality during the past 5.8 ka. We compare this record to a sedimentary ancient DNA (sedaDNA)-inferred vascular plant record from the same lake, aiming to overcome the uncertainty of plant community impacts on leaf waxes. As the sedaDNA record reveals a stable plant community after the colonization of Betula sp. at 6.1 ka, we interpret plant wax δ^2H values to reflect climate, specifically mean annual precipitation δ^2H . However, the distributions of n-alkanoic acid homologs suggest that aquatic mosses, which are not represented in the sedaDNA record, may become more abundant towards the present. Therefore, we cannot exclude the possibility that changes in the plant community cause changes in the plant wax δ^2H record, particularly long-chain waxes, which become less abundant through this record. We find that Lake Qaupat mid-chain plant wax δ^2H is enriched coincident with high Labrador Sea summer surface temperature, which suggests that local moisture sources in summer and early autumn have the greatest impact on precipitation isotopes in this region. © 2021 John Wiley & Sons, Ltd.

KEYWORDS: Baffin Island; moisture sources; paleoclimate; plant wax $\delta^2 H$; precipitation seasonality

Introduction

Projected increases in Arctic precipitation and plant community response

Increased precipitation in the Arctic is a robust response to surface warming, and this feature is particularly strong over the eastern North American Arctic (Collins et al., 2013; Bintanja and Selten, 2014; Overland et al., 2014; Anderson et al., 2018). Models run using the IPCC RCP 8.5 scenario predict that by 2100 CE the Arctic will become 10-20% wetter in the summer, spring and autumn via increased poleward moisture transport and higher specific humidity in the troposphere, and up to 50% wetter in the winter, via increased local evaporation over warmer, newly icefree Arctic seas (Collins et al., 2013). On Baffin Island, increased winter precipitation is largely sourced from Baffin Bay, over which models project a 50% increase in surface evaporation due to a 25-30% decrease in seasonal sea ice cover (Bintanja and Selten, 2014). Since this increase in precipitation across all seasons is coincident with increased temperatures, it is probable that much of this additional precipitation will fall as rain (Collins et al., 2013; Bintanja and Andry, 2017).

Increased summer precipitation and higher temperatures in the Arctic have global significance. Enhanced summer warmth and rainfall on the Greenland Ice Sheet and Canadian polar ice caps cause more negative mass balance, contributing to sea level rise (van den Broeke *et al.*, 2009; Fettweis *et al.*, 2013). In lower elevation regions, longer plant growing season and the expansion of low-lying shrubs into higher latitudes reduces surface albedo and adds water vapor to the atmosphere (Sturm et al., 2005; Swann et al., 2010; Loranty et al., 2011), both of which further enhance surface warming. Warmer and wetter Arctic summers also facilitate the expansion of wetlands that release methane, amplifying atmospheric greenhouse gas concentrations (Sturm et al., 2005; Miller et al., 2010; Loranty et al., 2011). Most of our understanding of these mechanisms is based on a short, sparse observational record spanning recent decades. Studying the response of Arctic precipitation seasonality and plant communities to past warm periods can provide further insights into the relationship between these mechanisms on longer time scales and under conditions that are partially analogous to the changes occurring today.

The importance of precipitation seasonality and source to water isotope proxies

Moisture sources to the Arctic vary seasonally and are important to constrain, as they can strongly influence the isotopic composition of precipitation (Sodemann *et al.*, 2008; Putman *et al.*, 2017). While no moisture source studies of Baffin Island presently exist, south-western Greenland may provide a reasonable analog. Today, precipitation that falls on south-western Greenland in the summer is predominately from low- and midlatitude sources, such as the tropical Atlantic Ocean and North America (Nusbaumer *et al.*, 2019; Cluett *et al.*, 2021). Autumn, winter and spring precipitation on Greenland tend to have more high-latitude, local origins, such as the Labrador Sea, Baffin Bay

*Correspondence: Devon B. Gorbey, as above. E-mail:devongor@buffalo.edu

¹Department of Geological Sciences, University at Buffalo, Buffalo, NY, USA

²Department of Geological Sciences and Institute of Arctic and Alpine Research, University of Colorado Boulder, Boulder, CO, USA

³Department of Ecology and Evolutionary Biology, University of California Santa Cruz, Santa Cruz, CA, USA

⁴Institute of Arctic Biology, University of Alaska Fairbanks, Fairbanks, AK, USA

⁵Department of Geosciences, Smith College, Northampton, MA, USA

and the North Atlantic Ocean This seasonal moisture source variability is caused by seasonal differences in atmospheric circulation (Bintanja and Selten, 2014; Dufour et al., 2016; Singh et al., 2017). In the summer, when air temperature is highest, humidity and resulting precipitation in the Arctic increases per the Clausius-Clapeyron relationship, which describes the relationship between temperature and atmospheric water vapor pressure. The fraction of poleward moisture transport increases due to this increased air temperature and weaker blocking between high and low latitudes (Bintanja and Selten, 2014; Dufour et al., 2016). Local moisture becomes a more important source of precipitation in the winter because the jet stream flows faster and is farther south, resulting in stronger blocking between the Arctic and mid-latitudes. A warmer Earth, therefore, results in more Arctic precipitation in all seasons via (i) increased local evaporation from local, ice-free seas, (ii) reduced winter blocking in the Arctic via a weaker temperature gradient between low and high latitudes, and (iii) increased poleward moisture transport in the summer (Hurrell and Deser, 2010; Bintanja and Selten, 2014; Dufour et al., 2016; Singh et al., 2017).

Water isotope proxies are commonly used to understand changes in precipitation source and seasonality through time. Low-elevation Arctic regions are growing in importance for paleoclimate research as isotope and geochemical proxies are developed and deployed in lacustrine, paleosol and coastal marine archives (Konecky *et al.*, 2020). Moisture source and isotope modeling for coastal western Greenland suggests that precipitation isotopes in these regions are sensitive to changes in moisture source and to local temperature (Cluett *et al.*, 2021). Proxy records in these regions can therefore be useful to describe changes in moisture sources associated with seasonal and long-term global climate changes, as described above.

One powerful proxy for water isotopes is the δ^2H value of plant waxes, which are ubiquitous in lake sediments (Castañeda and Schouten, 2011; Sachse et al., 2012). Plant wax δ^2 H reflects the δ^2 H value of the plant source water, but can be modified by processes including evaporation and apparent fractionation, which vary between plant functional types (Sachse et al., 2012). Modern global calibrations suggest a strong relationship between $\delta^2 H$ of precipitation and plant wax $\delta^2 H$, despite large apparent fractionation uncertainties (Sachse et al., 2012; McFarlin et al., 2019). Additionally, waxes derived from plants in different habitats can reflect different source waters (Thomas et al., 2020). Aquatic plants, which generally produce midchain waxes (Gao et al., 2011), use lake water to produce plant waxes, and therefore reflect the seasonality of lake water. Terrestrial plants, which tend to produce long-chain waxes, use soil water, which usually reflects growing season precipitation (Lamhonwah et al., 2017). Furthermore, terrestrial plant leaf water is more susceptible to evaporative enrichment than aquatic plant leaf water (Sachse et al., 2012), as submerged aquatic plants are not directly exposed to the atmosphere. Therefore, terrestrial plant waxes reflect growing season precipitation and evaporative enrichment, while aquatic plant waxes reflect the isotopic composition of lake water, which is affected by residence time, evaporation, runoff and precipitation seasonality (Shuman et al., 2006; Rach et al., 2017; Thomas et al., 2020). A strong understanding of all the above variables is critical to accurately interpret paleoclimate records. Modern lake water residence time, precipitation seasonality and plant community are well constrained at Lake Qaupat, making it an ideal location to study paleoclimate in southern Baffin Island, where no other Holocene precipitation isotope records presently exist. Therefore, this study fills a gap in quantifying precipitation source and seasonality changed under past climate changes.

We present a plant wax δ^2H record from Lake Qaupat (QPT, informal name, 63.677°N, 68.198°W, 35 m above sea level) on Baffin Island, Nunavut, Canada (Fig. 1), to evaluate changing amount-weighted mean annual precipitation δ^2H (hereafter, mean annual precipitation δ^2H) and terrestrial plant water δ^2H during the past 5.8 ka. We present this plant wax δ^2H record alongside an existing vascular plant sedimentary ancient DNA (sedaDNA) dataset (Crump et al., 2019) from an adjacent sediment core and regional temperature and sea ice records. We use these Holocene climate records to assess the following: (i) whether changes in the vascular plant community affect the plant wax δ^2H record, and (ii) the relationship between temperature, sea ice and precipitation δ^2H and their implications for moisture sources to Baffin Island through the Holocene.

Methods

Study area

Lake QPT is a small lake (8.2-ha surface area, maximum depth of 9.2 m) that is 18 km south-west of Iqaluit, Nunavut, within a large, 15-km² catchment (Fig. 1). The lake and catchment were occupied by the Laurentide Ice Sheet until around 9–8 ka, after which the lake received decreasing silt-laden meltwater as the Laurentide Ice Sheet retreated northward and relative sea level fell (Miller, 1980). Organic-rich sedimentation increased until around 5.8 ± 0.1 ka at which point minerogenic silt deposition in the basin declined dramatically. Today, the lake is fully flushed by summer precipitation each year. We calculate the residence time (average time a given molecule of water remains in the lake) for the ice-free season at Lake QPT to be about 1 month using the following equation (Jonsson et al., 2009):

Residence Time $= \frac{Lake\ Volume(m^3)}{Catchment\ Area(m^2)\ *\ Summer\ Precipitation(m)}$

where lake volume is approximated based on bathymetric measurements taken during coring activities, the catchment area is measured using ArcticDEM and summer precipitation is measured at the Iqaluit Airport (Environment Canada) (Fig. 2). Today, Lake QPT has one major inflow that is hydrologically connected to several other lakes in the catchment and flows throughout the summer, and one outflow to Frobisher Bay (Fig. 1).

Today, precipitation that falls in the QPT catchment on southern Baffin Island is probably from a combination of local (Frobisher Bay and the Labrador Sea) sources and lower latitude distal sources, including the North Atlantic Ocean and North America (Sodemann et al., 2008; Bintanja and Selten, 2014; Dufour et al., 2016; Nusbaumer et al., 2019). Southern Baffin Island is coolest and driest in the winter months (December-March), when average temperatures are between -20 and -30 °C, and 10-15 mm of precipitation falls monthly (Fig. 2). Southern Baffin Island is warmest and wettest from June to September, when temperatures range from 5 to 10 °C and 30-50 mm of precipitation falls monthly. Precipitation is most ²H-depleted in the winter (November to May; –178‰, amount weighted) and most ²H-enriched in the summer (June to October; -103‰, amount weighted). In total, 60% of the annual precipitation falls between June and October, when lakes are ice-free, as inferred from satellite

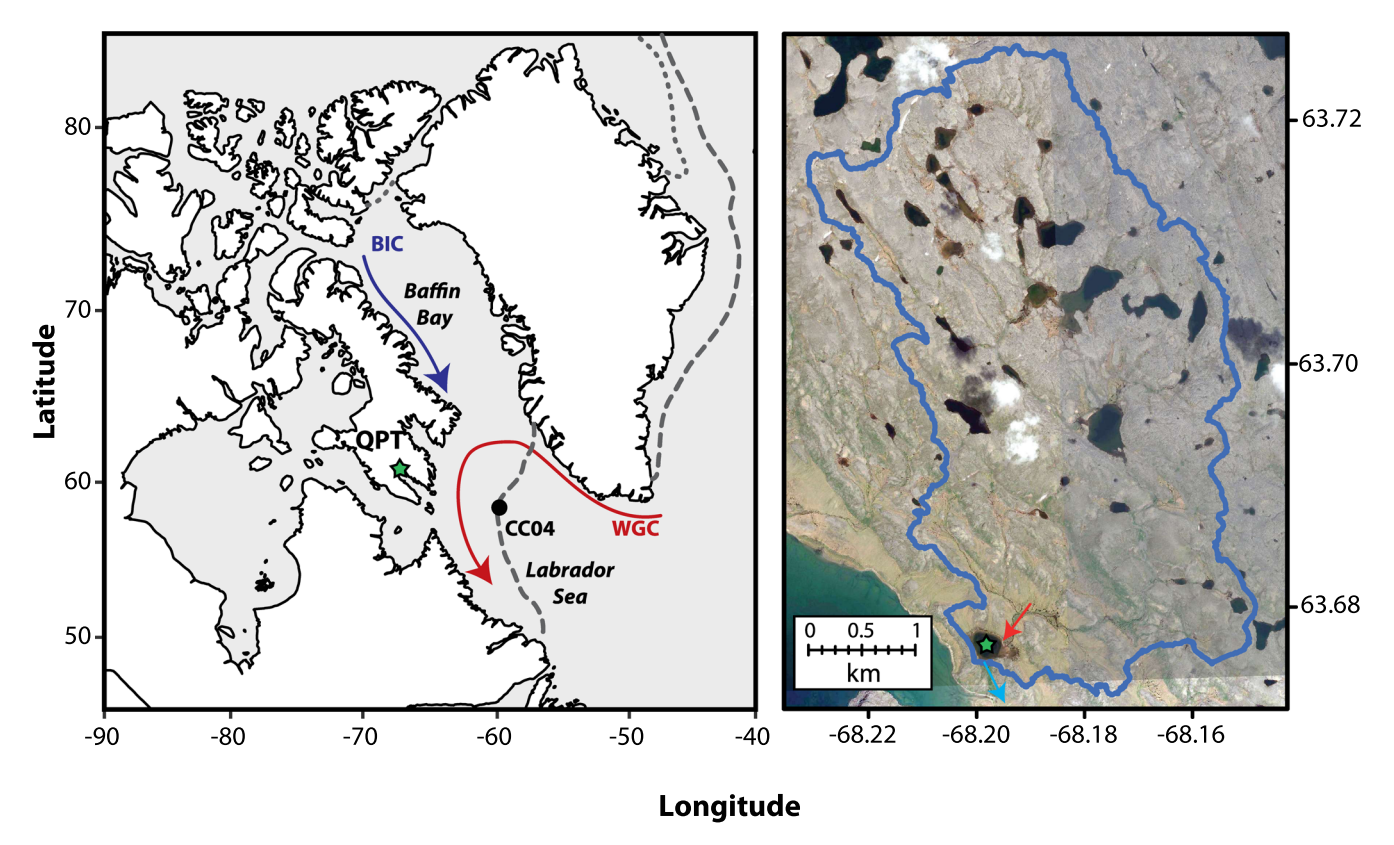


Figure 1. Left: site map showing the location of Lake Qaupat (green star) on Baffin Island and Labrador Sea sediment core CC04 (black circle; Gibb *et al.*, 2015). The West Greenland Current (WGC) is shown in red and the Baffin Island Current (BIC) is shown in blue. The dashed and dotted grey lines reflect the modern winter and summer sea ice fronts, respectively (1981–2010 average; National Snow and Ice Data Center, 2018). Right: Lake Qaupat catchment boundary map (blue outline) and core site location (green star). Inflow and outflow streams are marked in red and cyan, respectively. [Color figure can be viewed at wileyonlinelibrary.com]

imagery. Thus, amount-weighted mean annual precipitation $\delta^2 H$ (–133‰) is slightly biased towards summer precipitation $\delta^2 H$ (Fig. 2) (Bowen and Revenaugh, 2003; IAEA/WMO, 2015; Bowen, 2017).

Modern surface lake water isotope samples from Lake QPT fall between -125 and -130% δ^2 H, indicating that, when the samples were collected in summer, the isotopic composition of the lake water reflected amount-weighted mean annual precipitation isotopes (Fig. 2). The lake's short residence time, however, suggests that during summer if the lake is flushed only by summer precipitation, the lake water should be biased towards summer precipitation isotope values. The isotopic composition of the inflow stream in mid-August is -130% δ^2 H, i.e. 2 H-depleted compared to summer precipitation $\delta^2 H$, perhaps because snow continues to melt throughout the summer and mixes with ²Henriched summer precipitation. It is also possible that the lakes in the QPT catchment that drain into Lake QPT's inflow (Digital Globe) contribute water that has isotope values similar to amountweighted mean annual precipitation, similar to lakes throughout southern Baffin Island (Sauer, 1997). Lake water deuterium excess values are close to precipitation deuterium excess values (Fig. 2), indicating that Lake QPT experiences minimal evaporative

Today, aquatic mosses are the most abundant aquatic plant species within Lake QPT (>7% of lake area, measured from Digital Globe imagery). Several emergent aquatic plant species grow in low abundances along the shallow margin of the lake. Within 50 m of Lake QPT (56 826 m²), low-lying shrubs including *Betula nana* and *Salix arctica* are the most abundant terrestrial plant species (covering ~7 and 6% of the catchment area within 50 m of the lake shore), though 10% of the land within 200 m of Lake QPT is barren.

Core subsampling and age model

We collected sediment cores through lake ice in spring 2016 using a modified Nesje piston coring system (Nesje, 1992). We collected two adjacent cores (QPT16-2A and QPT16-3A) from the center of the lake at 8.8 and 9.2 m water depth, respectively, and kept them in 4 $^{\circ}\text{C}$ cold storage at the University of Colorado Boulder until subsampling. Both cores had intact sediment–water interfaces.

We split and subsampled QPT16-2A in a *sed*aDNA clean laboratory at Curtin University for *sed*aDNA and radiocarbon analyses. The methods for those analyses are detailed in Crump *et al.* (2019). We split and subsampled QPT16-3A at the University of Colorado for plant wax and radiocarbon analyses. We collected magnetic susceptibility data at 0.3-cm resolution from the archive half of QPT16-3A at the University of Minnesota LacCore facility using a point sensor on a Geotek core logger and at 5-cm resolution on the whole core QPT16-2A at CU Boulder using a loop sensor.

We use the chronological constraints (six radiocarbon ages from each core QPT16-2A and QPT16-3A) presented in Crump *et al.* (2019). To plot proxies with age model uncertainty, we generated a new age–depth model in GeoChronR (McKay *et al.*, 2020) using the chronological constraints from Crump et al (2019) and Bacon v. 2.5.1 software (Blaauw and Christen, 2011) with IntCal13 (Reimer *et al.*, 2013). For the model, we set section thickness at 5 cm and mean accumulation rate for the prior at 10 years cm $^{-1}$. Although this age model is based on age constraints from both QPT16-2A and QPT16-3A, the ages assigned to the plant wax δ^2 H values that we focus on in this study are from QPT16-3A, and would be similar if we only used age constraints from QPT16-3A. The chronological constraints and age–depth

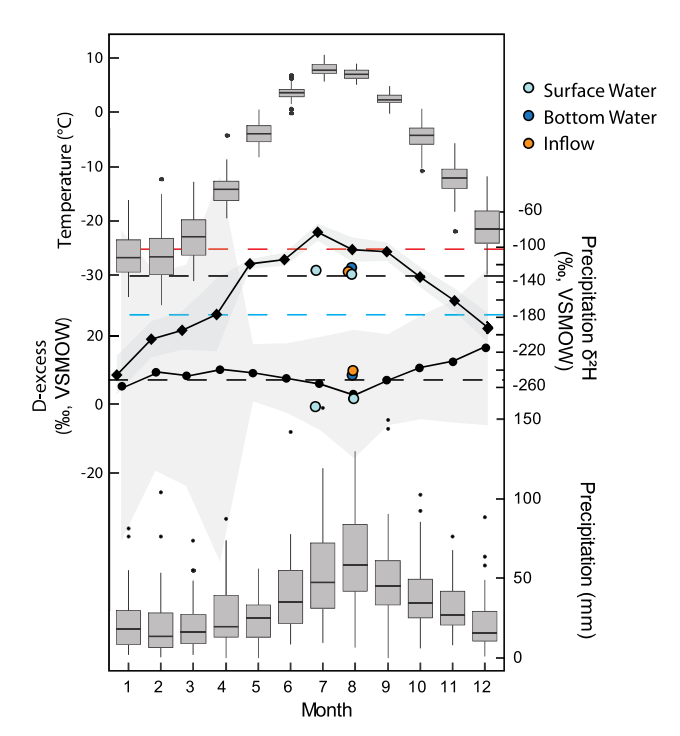


Figure 2. Modern climate on southern Baffin Island. From top to bottom: 1946–2007 monthly average temperature measured at Iqaluit Airport (Environment Canada); modeled monthly precipitation $\delta^2 H$ at Lake QPT with 2 sigma uncertainty; and d-excess with 1 sigma uncertainty (Bowen and Revenaugh, 2003; IAEA/WMO, 2015; Bowen, 2017). 2018 surface water, bottom water and inflow water isotope samples are plotted in light blue, dark blue and orange, respectively (analytical errors on water isotope measurements are smaller than the dots). Dashed lines reflect amount-weighted mean annual (black), summer (red) and winter (cyan) precipitation $\delta^2 H$ values at Lake QPT; 1946–2007 monthly total precipitation (Environment Canada). Box plots: lines are median values, boxes are quartiles, whiskers are 95th percentiles and black dots are outliers. [Color figure can be viewed at wileyonlinelibrary.com]

model are available at https://www.ncdc.noaa.gov/paleo/study/34352.

We also used GeoChronR to calculate statistical ensemble correlations between our Lake QPT data with an existing dataset from the Labrador Sea (Gibb $et\ al.$, 2015). We incorporated age model uncertainty for both records, and calculated the fraction of significant correlations between the plant wax isotope records and Labrador Sea summer surface temperature (described in the Results), winter surface temperature and monthly sea ice cover. For each statistical test, we conducted an isospectral comparison, which accounts for autocorrelation, with 250-year bins (McKay $et\ al.$, 2020). We also include the false discovery rate, which minimizes the risk of over-inflating significance that may occur because of running the same test many times on the data. We consider two datasets to be robustly correlated within age certainty if more than half of the ensemble correlations are significant above the 95% confidence interval (p < 0.05; McKay $et\ al.$, 2020).

Downcore plant wax purification and analysis

We extracted lipids from freeze-dried sediment at 5-cm resolution using a Dionex 200 Accelerated Solvent Extractor with 9: 1 (v/v) solution of dichloromethane (DCM) and methanol in the CU Boulder Earth Systems Stable Isotope Laboratory. We then purified and analyzed plant waxes in the University at Buffalo Organic Stable Isotope Biogeochemistry Laboratory. We separated compounds in the total lipid extract into acid and neutral fractions by eluting the polar fractions with a 2: 1 (v/v) solution of DCM/isopropanol and by eluting

the acid fractions through NH_2 bondesil flash columns with a 4% solution of acetic acid in DCM. We methylated the acid fractions overnight at 60 °C in a solution of 2% HCl in methanol. We isolated the methylated acid fractions by eluting each sample using DCM through silica gel flash columns.

We quantified the fatty acid methyl esters (FAMEs) using a Thermo Trace 1310 gas chromatograph (GC) equipped with two flame ionization detectors (FID), AI 1310 autosamplers and two 30-m HP-1MS fused silica columns. We injected samples using split/splitless injectors held at 250 °C, operated in splitless mode at a flow rate of 14.0 ml min⁻¹ for 0.75 min. We held column flow at a constant rate of 3.60 ml min⁻¹ using hydrogen carrier gas. We held the oven at an initial temperature of 60 °C for 1 min, then ramped to 220 °C at 20 °C min⁻¹. We then ramped the oven to a final temperature of 315 °C at 6 °C min⁻¹, and held the final temperature for 10 min. Peaks were identified by retention time, using an internal monounsaturated *cis*-eicosenoic FAME standard as a reference. We calculated FAME concentrations using external calibration curves established for C₂₀ and C₂₈ FAMEs.

We used these FAME concentrations to dilute and inject target amounts of compounds on a Thermo Delta V + isotope ratio mass spectrometer (IRMS), equipped with a split/splitless injector and a TriPlus RSH autosampler, connected to the IRMS via IsoLink II and Conflo IV. We used the same GC-FID conditions and programs as those used during FAME quantification, except that we used helium carrier gas at a flow rate of 1.50 ml min⁻¹. We ran samples in triplicate (or in duplicate for small samples), and ran internal standards (C_{20} and C_{28} FAMEs) after every second sample to correct for peak size linearity and to calibrate to the Vienna Standard Mean Ocean Water (VSMOW) scale. We analyzed standards (C₁₈ and C₂₄ FAMEs) at the beginning and end of each IRMS run to correct for drift. We corrected FAME δ^2 H for the hydrogens added during methylation with palmitic acid of known isotopic composition (Lee et al., 2017). We determined total analytical uncertainty as the square root of the sum of the squares of uncertainty in the drift, linearity and methanol-derived hydrogen corrections. We combined this total analytical uncertainty with the standard deviations from replicate analyses, and express this uncertainty as the standard error of the mean (SEM). The SEM values from samples within gyttja are between 2 and 5% for C22 FAMEs and between 2 and 2.5% for C_{28} FAMEs. The SEM values from samples within the clastic sediments are higher, between 2.5 and 11% for C22 FAMEs and between 2 and 3.5% for C₂₈ FAMEs. All biomarker data for these analyses are freely available at the NOAA/World Data Service for Paleoclimatology website: https://www.ncei. noaa.gov/access/paleo-search/study/34352.

Several samples in the earliest part of the QPT16-3A record had low FAME yields. In these cases, we analyzed additional samples from QPT16-2A to extend the plant wax record. All the QPT16-2A samples were collected within the clastic unit. While some of these data are shown in subsequent figures, we do not interpret these data to reflect shifts in climate.

Modern plant wax purification and analysis

We report *n*-alkanoic acid relative abundance data from modern plant samples from the Lake QPT catchment, including *Hippuris vulgaris*, an emergent aquatic plant, and shrubs *Betula nana* and *Salix arctica*, which are abundant in the modern QPT catchment and present in the plant community through most of Lake QPT's history (Crump *et al.*, 2019). We also present *n*-alkanoic acid relative abundance data from an average of four individuals of submerged aquatic moss (*Scorpidium revolvens* and *Calliergon* sp.) collected from more northern sites on Baffin Island

(Brother-of-Fog Lake: $67.19 \,\text{N}$, $63.17 \,\text{W}$, n=1; Windy Lake: 66.84 N, 63.81 W, n=1; Lake AFR: 72.39 N, 77.53 W, n=2). We froze plant samples until time of processing at the University at Buffalo. We extracted lipids from freeze-dried plant leaves using methods modified from Freimuth et al. (2019) and Longo et al. (2013). We first sonicated the leaves in a 9: 1 solution of DCM/ methanol (v/v) for 15 min three times, pipetting solvent into a new vial after each sonication. We then saponified the esters by adding 1 ml of a 1 M solution of potassium hydroxide in methanol to the dried-down total lipid extract and placing each sample on a 65 °C hot plate for 3 h. After the samples returned to room temperature, we conducted three hexane extractions, using a 5% salt water solution to aid separation and shaking the vials between extractions. Upon completion of these hexane extractions, we purified the n-alkanoic acids using LC-NH2 columns with three elution steps: three column volumes of hexane preceded the same two steps as for the sedimentary waxes. After this LC-NH₂ column step, we methylated the acid fraction and analyzed modern plant n-alkanoic acids via the same methods as sedimentary plant waxes.

Bulk geochemistry

We conducted total organic carbon (TOC), total nitrogen, and bulk δ¹³C analyses at the University of Colorado Boulder Earth Systems Stable Isotope Lab. We analyzed homogenized, freeze-dried sediment on a Thermo Flash Organic Elemental Analyzer (EA) connected to a Delta V+IRMS via Conflo IV. We combusted samples at 1020 °C and ran the samples through a normal phase gas chromatography column using helium carrier gas at a flow rate of 100 ml min⁻¹ in the EA, then 2 ml min⁻¹ in the IRMS. We removed carbon monoxide and water from the sample with a copper reduction column and a drying agent, respectively. We ran a low organic soil standard after every sixth sample to correct for linearity and drift. We used a high organic soil standard for monitoring and an external standard (Pugel) to establish a reference point for $\delta^{13}C$. The absolute uncertainty for $\delta^{13}C$ measurements is 0.14‰ and the C:N uncertainty is 3.2%, determined using repeat analyses of the standards analyzed throughout these sequences.

Modern lake water isotope analysis

We collected samples during 2018 and 2019 field campaigns in 4-ml vials with minimal headspace, sealed with Parafilm and kept cold until the time of processing. Samples were subsequently analyzed at the Organic and Stable Isotope Biogeochemistry Laboratory at the University at Buffalo. Samples were filtered at 0.22 μm and analyzed on a Picarro L2130-i Cavity Ringdown Spectrometer. Our sequence organization and correction procedures follow those outlined by van Geldern and Barth (2012). We injected each sample four times with the first replicate discarded, corrected for memory and drift, then normalized to VSMOW scale using five secondary isotope standards calibrated to the VSMOW-GISP-SLAP scale. We used a secondary standard of known value for quality control. Replicate uncertainty was better than 0.03% for $\delta^{18}O$ and 0.08% for $\delta^{2}H$.

Results

Plant wax concentration in sediment and relative abundance over time

The oldest samples in this dataset were collected from silty, clastic sediment rather than gyttja, as indicated by magnetic susceptibility data (Supporting Information, Fig. S1) and described in Crump et al (2019). The contact between clastic

sediment and gyttja is graded (Fig. S1). The sediments reflect local, organic deposition starting at 83 cm composite depth (corresponding to 5.8 ± 0.1 ka on our age model), when magnetic susceptibility reaches the average value for the upper 80 cm composite depth (Fig. 1). We present data from the silty, clastic layers in Fig. S2, but interpret only the plant waxes after 5.8 ± 0.1 ka to reflect a climate signal. Plant wax input to QPT sediments was influenced by marine and glacial clastic sediment before 5.8 ka, which we infer from the following lines of evidence: first, higher clastic content in the cores was probably derived from slope wash of glacial and marine sediments that were deposited during and after glaciation, before the basin was fully isolated due to isostatic rebound (Miller, 1980). Higher turbidity would have limited aquatic primary productivity. Second, *n*-alkanoic acid concentrations are low but highly variable from this portion of the record, ranging from 3 to 240 ng C_{28} g⁻¹ sediment and from 0.5 to 70 ng C_{22} g⁻¹ sediment over short (<100 years) time intervals (Fig. S2). This is a larger range of concentrations than in the upper 83 cm composite depth of this core, in which concentrations gradually increase with highest concentrations $(53 \text{ ng C}_{22} \text{ g}^{-1} \text{ sed}, 67 \text{ ng C}_{28} \text{ g}^{-1} \text{ sed})$ in the most recent part of the record (Fig. S2). Moreover, the n-alkanoic acid relative distributions are highly variable before 5.8 ka (Fig. 3). Combined with the presence of clastic material, we suggest that this large variability may indicate reworking of material on the landscape and/or variability in wax sources. Finally, the sedaDNA-inferred plant community is relatively stable after the colonization of Betula sp. at 6.1 ka (based on the updated age model from Crump et al., 2019). We therefore infer that plant wax sources to Lake QPT sediments stabilized shortly after organic sediment deposition began, around 5.8 ka. Accordingly, we only interpret plant wax $\delta^2 H$ data from the gyttja section (upper 83 cm composite depth, the past 5.8 ± 0.1 ka) of the core.

From 5.8 to 4.0 ka, C_{24} , C_{26} and C_{28} are the most abundant homologs in the record, after which C_{28} gradually becomes 10% less abundant than the average for 5.8–4.0 ka, and C_{22} and C_{24} become more abundant towards the present (Fig. 3). C_{26} is the dominant homolog before 1.2 ka (~30%), but in the past millennium C_{24} was the most abundant (~35%). The C_{20} and C_{30} homologs make up <10% of the relative abundance throughout the past 5.8 ka (Supporting Information, Fig. S2), so we focus our interpretation on the more abundant homologs.

Modern plant n-alkanoic acid distributions

We generated a dataset of modern plant n-alkanoic acid distributions to establish a baseline for interpreting the distribution of *n*-alkanoic acids downcore (upper panel of Fig. 3). Hippuris vulgaris, an emergent aquatic plant that covers <0.01% of the Lake QPT area, produces more C₂₈ than other *n*-alkanoic acids (42% relative abundance), which is consistent with the distribution of *n*-alkanoic acids in *Hippuris* vulgaris in other studies (Gao et al., 2011; Dion-Kirschner et al., 2020; Fig. 3). As we do not have an aquatic moss sample from Lake QPT, we measured the distributions of *n*-alkanoic acids from aquatic moss samples collected at three lakes in central and northern Baffin Island and report the average distribution of those samples here. All four of these samples contain similar wax relative abundances, dominated by the C_{24} n-alkanoic acid (31% of total waxes, SD = 3%; Fig. 3), and contain similar distributions to aquatic moss samples on western Greenland (Thomas et al., 2016), suggesting that aquatic mosses throughout this region have consistent n-alkanoic acid distributions, and the samples that we measured are probably representative of the mosses in Lake

QPT. We also measured wax relative abundances in the most abundant terrestrial plants in the Lake QPT catchment, two shrub species, as terrestrial plants can contribute significant amounts of waxes to lake sediments (Sachse *et al.*, 2012; Freimuth *et al.*, 2019; Dion-Kirschner *et al.*, 2020). The *Betula nana n*-alkanoic acid distribution is dominated by C_{22} (35%) in all three samples, whereas the *Salix arctica n*-alkanoic acid distribution is dominated by C_{26} (39%), though the C_{24} and C_{28} *n*-alkanoic acids also make up >20% of the wax production (Fig. 3).

We also report the absolute concentration of n-alkanoic acids in modern plants per gram of dry biomass sampled (Fig. 3; Table 1). Modern aquatic mosses produce the greatest amount of C_{24} , but *Betula nana* produces the greatest amount of C_{22} per gram of biomass. *Hippuris vulgaris* produces the greatest amount of C_{26} and C_{28} per gram of biomass. We use

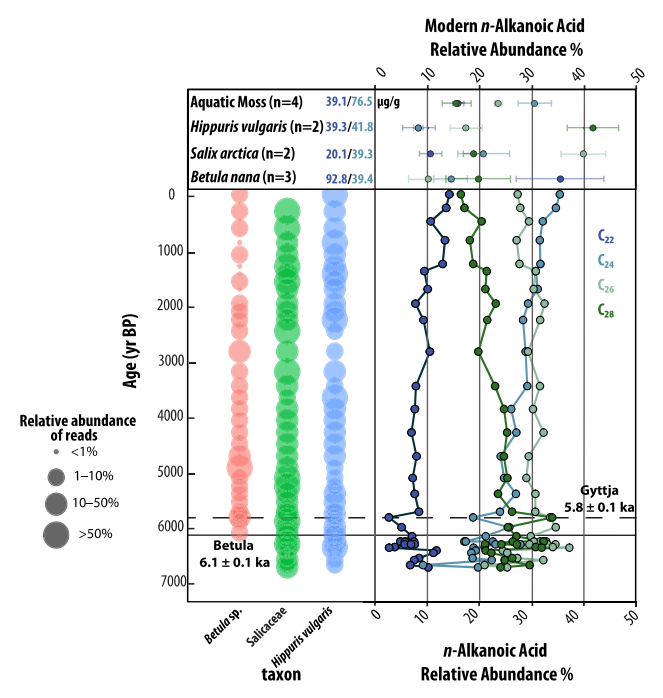


Figure 3. Top: Relative distributions of n-alkanoic acids of modern plants within the QPT catchment (note that mosses are from lakes throughout Baffin Island). Numbers to the right of the plant names detail the mass (μ g) of C_{22} (dark blue) and C_{24} (light blue) n-alkanoic acids produced per gram of biomass sampled. Left: relative abundance of sedaDNA metabarcoding reads for selected taxa (Crump et al., 2019). Right: relative distributions of n-alkanoic acids in Lake QPT sediment. Relative abundances were calculated such that all even-chain-length n-alkanoic acids from C_{20} to C_{30} sum to 100. C_{20} and $C_{30}n$ -alkanoic acids are present only at low abundances (Fig. S2) and are excluded from this figure. Dashed horizontal line at 5.8 ka marks the transition from clastic sedimentation to gyttja; solid horizontal line at 6.1 ka marks the first appearance of Betula sp. in the sedaDNA record based on updated age model. [Color figure can be viewed at wileyonlinelibrary.com]

these modern plant wax distributions to guide interpretations of general plant (terrestrial or aquatic) wax source changes through time (see Discussion).

Mid- and long-chain $\delta^2 H_{wax}$ at Lake QPT during the past 5.8 ka

Throughout the past 5.8 ka, C_{28} *n*-alkanoic acid δ^2 H, with a mean value of -124.5%, is consistently ²H-enriched relative to C_{22} *n*-alkanoic acid δ^2 H, which has a mean value of -147.5% (Fig. 4). The δ^2 H values of C_{22} and $C_{28}n$ -alkanoic acids are most variable from 5.8 to 4.5 ka, where C22 becomes \sim 20% ²H-depleted from \sim 236 to \sim 253% between 5.5 and 4.9 ka, followed by a 10 $^{\circ}$ H-enrichment to -245% by 4.1 ka (Fig. 4). C_{28} *n*-alkanoic acid δ^2 H shows a larger fluctuation from -220% at 5.2 ka to -250% at 4.9 ka, before recovering back to -220% at 4.6 ka. During the past 4.1 ka, C_{28} and C_{22} n-alkanoic acid δ^2 H varied by about 15‰, with no clear trend towards more enriched or depleted values in C22nalkanoic acid δ^2 H, and a decreasing trend in C_{28} n-alkanoic acid δ^2 H towards the present (Fig. 4). Throughout the record, we find that C_{22} and $C_{28}n$ -alkanoic acid δ^2H generally change in step with one another, although the isotopic difference between the two chain lengths ranges from 28% δ^2 H at 5.7 ka to <1% δ^2 H around 2.2 ka.

Bulk geochemistry

We use bulk elemental and stable isotope geochemical data to examine the mixing of terrestrial and aquatic plant contributions to Lake QPT bulk sediments during the past 5.8 ka (Fig. 4). Bulk sediment δ^{13} C fluctuates between ~-24 and -30% from 5.8 to 4.4 ka, after which it is stable around -26% until 1.1 ka (Fig. 4). Around 1.1 ka, δ^{13} C becomes 4% more 13 C-depleted, after which it gradually becomes enriched to -26% in the uppermost sample (Fig. 4). The carbon/nitrogen ratio (C:N) increases from 11 to 13 between 5.8 and 1.6 ka, at which point there is a sharp increase to 20, and after that the record is highly variable. TOC decreases from 4 to 2% between 6 and 5.5 ka, after which we observe a gradual increase to 5% in the uppermost sample.

Discussion

Multi-proxy approach to interpret plant community shifts at Lake QPT

We interpret mid-chain (C_{22} , C_{24}) n-alkanoic acids to predominately reflect submerged aquatic plant wax production for several reasons. The QPT sedimentary n-alkanoic acid distribution after 5.8 ka is similar to the distribution in modern aquatic mosses on Baffin Island (Fig. 3). While *Betula nana* produces more C_{22} per gram of biomass than aquatic moss, we

Table 1. Absolute abundance of n-alkanoic acids per gram of biomass ($\mu g g^{-1}$ sed) from modern plants in the Lake QPT catchment, Baffin Island, Nunavut, Canada, and the standard deviation (SD) of replicate samples.

Species	C_{22} (µg g ⁻¹ sed)	C_{22} SD (µg g ⁻¹ sed)	C ₂₄ (μg g ⁻¹ sed)	C_{24} SD (µg g ⁻¹ sed)	C_{26} (µg g ⁻¹ sed)	C_{26} SD ($\mu g g^{-1}$ sed)	C_{28} (µg g ⁻¹ sed)	C ₂₈ SD (µg g ⁻¹ sed)
Betula nana $(n = 3)$	92.8	35.6	39.4	20.3	32.6	25.3	62.0	43.0
Salix arctica $(n = 2)$	20.1	0.8	39.3	3.5	77.6	20.0	36.9	5.4
Hippuris $vulgaris (n = 2)$	39.3	3.7	41.8	11.6	86.6	20.5	223.2	93.8
Aquatic moss $(n=4)$	39.1	12.1	76.5	31.6	76.5	31.6	39.9	18.9

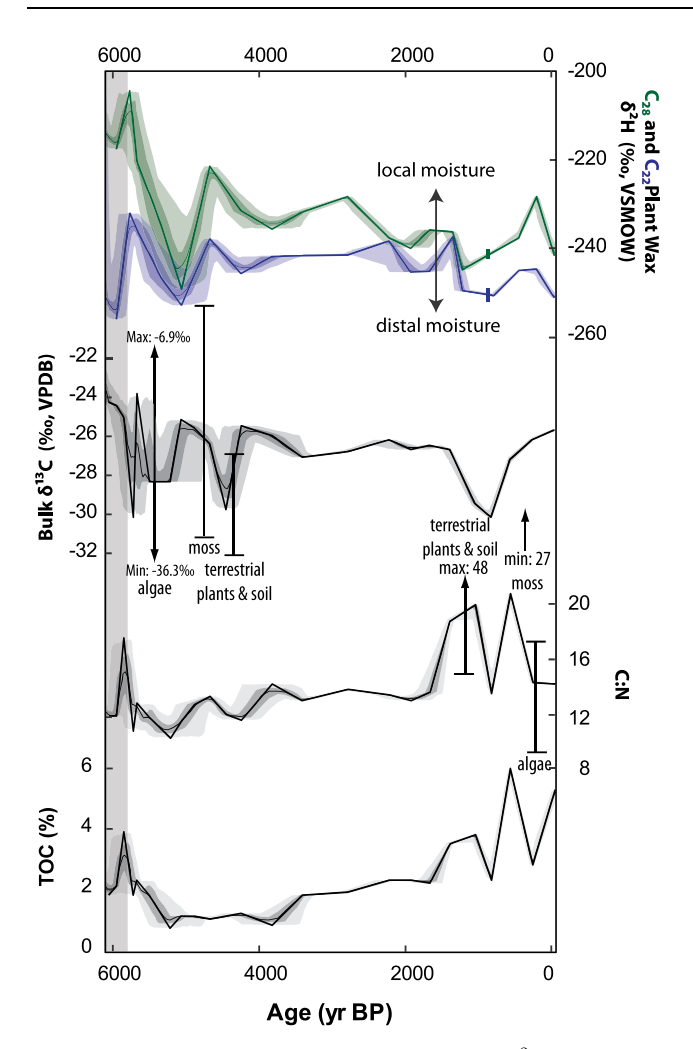


Figure 4. Top to bottom: C_{28} (green) and C_{22} (blue) $\delta^2 H$ (vertical bars represent mean standard error on isotope measurements) plotted with bulk sediment $\delta^{13}C$ values, bulk sediment C:N mass ratio, and total organic carbon (TOC). Vertical bars on the $\delta^{13}C$ and C:N plots indicate the range of values observed in modern Arctic vegetation (Blake, 1991; Florian *et al.*, 2015; Osburn *et al.*, 2019). For C:N, the modern ranges of terrestrial plants, soils and aquatic mosses are outside the range of axis limits. The bold line represents each record on the median age model, the fine line shows the median value of all age model iterations, and light and dark shading represent 1 and 2 sigma age model uncertainty, respectively. The gray shaded region indicates clastic sediment deposited in the earliest part of the record. [Color figure can be viewed at wileyonlinelibrary.com]

observe only a transient, minor decrease in the relative abundance of C22 following the establishment of Betula sp. in the QPT catchment at 6.1 ka (Crump et al., 2019; Fig. 3), suggesting that Betula sp. is at most only a minor source of mid-chain waxes to the QPT sediments. Moreover, C22 and C_{24} n-alkanoic acids have similar $\delta^2 H$ values and trends throughout the record (Fig. S2), suggesting they are probably from the same source. Finally, aquatic mosses grow within Lake QPT, and their waxes are probably more directly deposited and preserved in sediment than those from terrestrial plants. Indeed, mixing models of leaf waxes in another lake with high aquatic plant biomass suggest that aquatic plants can contribute large amounts of waxes to lake sediment (Gao et al., 2011), lending support to the interpretation that aquatic plants are a major source of n-alkanoic acids to Lake QPT sediments.

As modern lake water reflects amount-weighted mean annual precipitation (Fig. 2), we interpret the $C_{22}n$ -alkanoic acid δ^2H record to reflect changes in mean annual precipitation δ^2H . We examine this interpretation further by comparing

modern precipitation $\delta^2 H$ values to the uppermost leaf wax δ^2 H value in the Lake QPT record. We applied an apparent fractionation factor, which describes the isotopic offset between plant wax $\delta^2 H$ and meteoric water $\delta^2 H$, of -97%[median value with 5–95% confidence interval (CI) of –174 to -63%] (McFarlin *et al.*, 2019) to the C₂₂*n*-alkanoic acid δ^2 H value in the uppermost QPT sediment sample. This calculation yields a value of $-154 \pm 28\%$ (uncertainty calculated by propagating the 1σ analytical and replicate uncertainty for the plant wax $\delta^2 H$ sample and the 1σ uncertainty in the fractionation factor) for meteoric water δ²H inferred from C₂₂n-alkanoic acid, which is about 25% ²H-depleted relative to modern summer lake water $\delta^2 H$ values (-126 to -130%) and mean annual precipitation δ^2 H values (-133 ± 15‰; Fig. 2) (Bowen and Revenaugh, 2003; IAEA/WMO, 2015; Bowen, 2017). The measured and calculated values are within uncertainty, due to large uncertainties on the fractionation factor. Based on modern lake water isotope measurements and evidence that mid-chain waxes are derived from aquatic plants, we interpret the Lake QPT n-alkanoic acid δ^2 H record to reflect changes in mean annual precipitation $\delta^2 H$.

Long-chain (C₂₆, C₂₈) *n*-alkanoic acids are commonly interpreted to reflect terrestrial plant wax production (Sachse et al., 2012; Thomas et al., 2020). However, plant wax nalkanoic acid relative abundance data in Lake QPT sediments indicate that the C28n-alkanoic acid reflects a mixed aquatic and terrestrial source (Fig. 3). Three lines of evidence support this interpretation. First, the most abundant terrestrial plants in the QPT catchment (Salix arctica and Betula nana shrubs) produce mainly C_{22} or C_{24} and C_{26} *n*-alkanoic acid (Fig. 3). Second, the δ^2H value of $C_{28}n$ -alkanoic acid sometimes exhibits similar trends and sometimes different trends to the mid-chain waxes, suggesting that C28 and C22n-alkanoic acids reflect different plant sources to some degree. Third, we apply an apparent fractionation factor of -107% (median value with 5-95% CI of -153 to -44‰) (McFarlin et al., 2019) to convert the C_{28} *n*-alkannoic acid δ^2 H value in the uppermost Lake QPT sediment sample to precipitation δ^2H . The resulting leaf waxinferred precipitation $\delta^2 H$ value of $-135 \pm 33\%$ is similar to mean annual precipitation $\delta^2 H$ values. If $C_{28} n$ -alkanoic acid δ^2 H reflected a purely terrestrial plant signal, we would expect it to reflect summer, or growing season, precipitation $\delta^2 H$ (-103‰). In summary, as $C_{28}n$ -alkanoic acid δ^2H reflects a mixed plant source, we interpret the δ^2H value of this compound to reflect a mix of lake water (i.e. mean annual precipitation δ^2 H) and of terrestrial plant leaf water (i.e. summer precipitation $\delta^2 H$ and evaporation).

We compare Lake QPT *n*-alkanoic acid δ^2 H and relative abundance data to an existing sedaDNA record (Crump et al., 2019). This sedaDNA record shows a relatively stable plant community after the colonization of Betula sp. at 6.1 ± 0.1 ka (Crump et al., 2019). The n-alkanoic acid chain length distributions of modern Hippuris vulgaris and Salix sp. are similar to the distribution of sedimentary *n*-alkanoic acids early in our record, which may suggest that emergent aquatic and terrestrial plants were more represented in sediment early in the record. However, after 4.0 ka, sedimentary wax relative abundances are increasingly similar to aquatic moss wax abundances, and the distribution of sedimentary n-alkanoic acids in the uppermost two sediment samples closely resembles that of modern aquatic mosses (Fig. 3). We do not interpret this increase in aquatic C24n-alkanoic acids to reflect a decrease in terrestrial wax contribution to the record; rather, we interpret this change to reflect the development of the thick aquatic moss mats that we observe at the bottom of Lake QPT today. Therefore, this plant wax-inferred plant community shift does not contradict the sedaDNA-inferred vascular plant

community, as bryophytes are not well represented in the sedaDNA metabarcoding assay used (Taberlet et al., 2007). While we draw different conclusions about plant community shifts from leaf waxes and sedaDNA, these individual conclusions are not mutually exclusive but instead are complementary, resulting in a broader understanding of climatological and ecological change through time at Lake QPT. However, as the plant wax data suggest an increasing influence of aquatic mosses towards the present, we cannot exclude the possibility that vegetation shifts, as opposed to or in addition to changes in regional climate, influence the plant wax δ^2 H record to some degree.

While plant wax $\delta^2 H$ studies are useful in reconstructing δ²H of plant source water pools, it is important to consider plant community changes, which can cause changes in plant wax δ^2 H values via differences in apparent fractionation. Apparent fractionation describes the δ^2H fractionation during water uptake and plant wax synthesis, and results in plant wax δ²H becoming more ²H-depleted than its source water (Chikaraishi and Naraoka, 2003). As different plant species may have different apparent fractionation factors, changes in the plant community through time can cause changes in plant wax δ^2 H that are not directly due to climate change. We therefore examine whether major shifts in the vascular plant community, inferred from sedaDNA metabarcoding, appear to influence *n*-alkanoic acid relative abundance or δ^2 H. The relative abundance of sedaDNA reads is not a direct, quantitative proxy for the relative abundance of plant taxa on a landscape, due to biases inherent in the metabarcoding process. Rather, changes through time for a given taxon generally indicate the presence or absence of that taxon in the catchment. The most notable change in the vascular plant community at Lake QPT was the colonization of Betula sp. at 6.1 ± 0.1 ka (based on the age model update from Crump et al., 2019), after which the sedaDNA-inferred vascular plant community remained relatively stable. Thus, the relative n-alkanoic contribution of terrestrial plant waxes to sediment was probably constant after 6.1 ka. Due to changes in sediment and n-alkanoic acid sources discussed above (see Results), we only interpret the leaf wax record from 5.8 ka to the present. Moreover, apparent fractionation (ε_{app}) values for important terrestrial plant taxa within the Lake QPT catchment, compiled from other mid- and high-latitude regions (Hou et al., 2007; Gao et al., 2014; Daniels et al., 2017; Dion-Kirschner et al., 2020; O'Connor et al., 2020), are broadly similar (ε_{app} Shrubs = $-93 \pm 17\%$, n = 37; ε_{app} Herbs, including graminoids = $-96 \pm 29\%$, n = 9; Supporting Information, Table S1), suggesting that a change in the relative abundance of major plant species in the QPT catchment would not influence the QPT δ^2 H records simply via differences in apparent fractionation. Because the mid- to late Holocene terrestrial plant community was relatively stable at Lake QPT and apparent fractionation factors of dominant plants in the catchment are similar, the *n*-alkanoic acid plant wax $\delta^2 H$ values at Lake QPT probably primarily reflect changes in mean annual precipitation $\delta^2 H$, but we cannot completely exclude the possibility that vegetation shifts affect the plant wax $\delta^2 H$ signal to some degree.

Bulk elemental and stable isotope geochemical data provide a third perspective of biochemical change through time at Lake QPT. We plotted downcore C:N and bulk δ^{13} C with modern ranges of soil, terrestrial plant, moss and algae samples collected from north-eastern Baffin Island (Florian *et al.*, 2015), Ellesmere Island (Blake, 1991), western Greenland (Stevenson *et al.*, 2020) and south-western Greenland (Osburn *et al.*, 2019) to place geochemical changes in Lake QPT sediments in the context of modern vegetation (Fig. 4). We focus on the interval

after 5.8 ± 0.1 ka, once clastic sediment input had declined. The consistently low C:N in downcore sediments suggest that algal productivity is an important contributor of organic matter to sediment throughout the record relative to terrestrial plants, soils, and aquatic mosses, which generally have higher C:N than we observe downcore (Fig. 4). However, increasing C:N towards the present may reflect an increase in vascular plants or moss input over time. The δ^{13} C values generally fall within the range of all potential sources (Fig. 4; Blake, 1991; Florian et al., 2015; Osburn et al., 2019). TOC increases by 5% through our time series, indicating a general increase in primary productivity and/or increasing degradation with depth. Plant wax distributions, sedaDNA and bulk geochemical data primarily capture aquatic, terrestrial and algal productivity, respectively. Given the uncertainties in different proxies, it is important to use a multi-proxy approach to more holistically reflect the different processes within a lake system and to generate more robust climate interpretations. Taken together, we interpret these three paleovegetation datasets to reflect a general increase in primary productivity through time in the Lake QPT catchment, as soils become more developed and vascular plants and aquatic mosses become more established.

Inferring moisture source shifts from plant wax $\delta^2 H$ at Lake QPT

The $C_{28}n$ -alkanoic acid $\delta^2 H$ record at QPT, which probably reflects a mixed signal of terrestrial and aquatic plant waxes, shows a long-term, $20\%^2 H$ -depletion from 4.5 ka towards the present. The $C_{26}n$ -alkanoic acid $\delta^2 H$ record is similar (Supporting Information, Fig. S2). This shift occurs in step with regional climate cooling (Wolfe, 2003; Anderson *et al.*, 2008; Briner *et al.*, 2016; Pendleton *et al.*, 2017) and a 10% decrease in relative abundance of $C_{28}n$ -alkanoic acid in the Lake QPT sediment record (Fig. 3). Thus, it is challenging to determine whether the $C_{28}n$ -alkanoic acid became gradually depleted due to a catchment-scale vegetation shift towards greater aquatic moss or due to regional-scale climate change. Therefore, we do not interpret a climate signal from $C_{28}n$ -alkanoic acid $\delta^2 H$.

Instead, we primarily interpret shifts in regional climate using the C₂₂*n*-alkanoic acid record, which is probably primarily produced by aquatic plants throughout the past 5.8 ± 0.1 ka (section above). The QPT C_{22} *n*-alkanoic δ^2 H record (Figs. 4 and 5) suggests a period of relative moisture source stability on southern Baffin Island after the early Holocene, and more specifically, between 4.5 and 2 ka, despite widely observed progressive air temperature decline in the eastern North American Arctic after 6 ka (Wolfe, 2003; Anderson et al., 2008; Briner et al., 2016; Pendleton et al., 2017). Despite this regional atmospheric cooling, higher, stable temperatures in the Labrador Sea from 4.5 to 2 ka (Gibb et al., 2015) may have facilitated enhanced local moisture transport to Lake QPT. After 2 ka, a 10% depletion in C_{22} *n*-alkanoic acid δ^2 H could be explained by either a decrease in summer and autumn precipitation amount or greater isotope distillation, caused by relatively lower temperatures in the Labrador Sea (discussed further below) or lower air temperatures on southern Baffin Island. This late Holocene temperature decrease is reflected in records of glacier advances (Briner et al., 2009; Miller et al., 2013; Lecavalier et al., 2017). Although we do observe similarities between the Lake QPT record and regional climate, we acknowledge that increased wax contribution from aquatic mosses over time may also contribute to changes in the Lake QPT record.

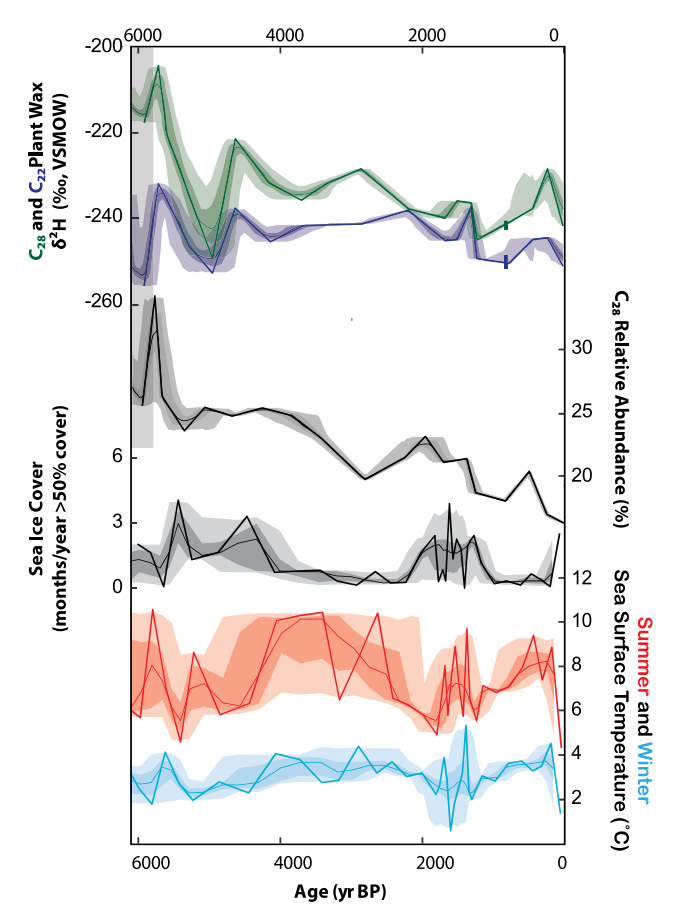


Figure 5. Top to bottom: C_{28} (green) and C_{22} (blue) n-alkanoic acid δ^2H (vertical bars represent standard error on isotope measurements) plotted with C_{28} relative abundance from Lake QPT and with Labrador Sea core CC04 dinocyst-inferred annual duration of sea ice cover (black) and late summer (red) and late winter (cyan) sea surface temperature (Gibb et al., 2015). The bold line represents each record on the median age model, the fine line shows the median value of all age model iterations, and light and dark shading represent 1 and 2 sigma age model uncertainty, respectively. The gray shaded region indicates clastic sediment deposited in the earliest part of the QPT record. [Color figure can be viewed at wileyonlinelibrary.com]

In the modern day, contributions to Arctic precipitation from local moisture sources increase in the winter (Singh et al., 2017; Nusbaumer et al., 2019; Cluett et al., 2021). Under warmer conditions in the Arctic, local moisture delivery increases proportionally more than distal moisture delivery (Bintanja and Selten, 2014; Singh et al., 2017), resulting in relatively ²Henriched precipitation (Putman et al., 2017). Therefore, increases in local moisture contributions, which primarily occur in the late autumn and early winter due to enhanced evaporation from warmer and/or newly ice-free seas (Bintanja and Selten, 2014), would probably cause mean annual precipitation isotope values to become relatively ²Henriched. As the Labrador Sea is probably an important moisture source to southern Baffin Island (Nusbaumer et al., 2019; Cluett et al., 2021), decreased autumn and winter sea ice extent and/or duration in the Labrador Sea may open up a local moisture source, which in turn would cause relatively ²H-enriched precipitation to drop in the winter, causing amount-weighted mean annual precipitation isotopes to become more ²H-enriched.

Although 70% of annual precipitation at Lake QPT falls in the summer and autumn, we might expect changes in winter precipitation to have the greatest impact on mean annual precipitation isotopes, as changes in distal moisture transport in the summer do not greatly impact precipitation isotopes (Cluett et al., 2021). Since autumn and winter precipitation isotopes can be influenced by seasonal sea ice duration and extent as well as by source region temperature, we compare Lake QPT C_{22} *n*-alkanoic acid δ^2 H data with a sea ice and sea surface temperature record from Site CC04 near the modern limit of winter sea ice in the northern Labrador Sea (Gibb et al., 2015, Figs. 1 and 5), which is probably the most local source of winter moisture to southern Baffin Island. Over the past 6 ka, sea ice cover in the Labrador Sea was highest from 6 to 4.5 ka and 2.5 to 1.5 ka (\sim 3 months year⁻¹) and relatively low (>1 month year⁻¹) in the intervening times. In the present, the Labrador Sea is covered with ice for <1 month of the year (Gibb et al., 2015). If changes in Labrador Sea ice extent or seasonal duration caused changes in mean annual precipitation δ^2H on southern Baffin Island, we would expect QPT C_{22} n-alkanoic acid δ^2 H to be relatively ²H-depleted when there was longer seasonal sea ice cover. While there are some broadly similar trends between the two records, they are opposite to what we would expect: $C_{22}n$ -alkanoic acid δ^2H is at times more ²H-enriched when there is longer sea ice cover over the Labrador Sea (e.g. between 6 and 5 ka, Fig. 5). Indeed, we observe no correlation between the CC04 sea ice cover or winter sea surface temperature records and the Lake QPT C22 n-alkanoic acid δ^2 H record. We therefore conclude that there is no strong relationship between sea ice cover in the Labrador Sea and mean annual precipitation $\delta^2 H$ in southern Baffin Island. Compared to modern monthly precipitation isotope values and amounts, we estimate that winters would need to be 250% wetter to cause the observed 15‰ ²H-depletion in C_{22} *n*-alkanoic acid δ^2 H between 2.1 ka and the present. As winter is the driest season in southern Baffin Island (15% of annual precipitation falls during the winter months; Environment Canada), it is reasonable to assume that relatively small changes in winter sea ice extent do not cause the required 250% increase in precipitation amount to result in the observed change in $C_{22}n$ -alkanoic acid δ^2H (Bintanja and Selten, 2014).

Although there are other sources of winter precipitation to Baffin Island, we would not expect them to influence our precipitation isotope record. North of Lake QPT (Fig. 1), Baffin Bay seasonal sea ice duration is stable through our study interval (Gibb et al., 2015), and therefore not likely to strongly influence moisture source variability on southern Baffin. The North Atlantic Ocean is probably an important winter moisture source to Lake QPT, as it is well beyond the winter sea ice extent (Nusbaumer et al., 2019; Cluett et al., 2021). As the Atlantic Ocean is distal to Lake QPT, moisture transported from this region experiences more isotopic distillation than local moisture sources, so it is probably more ²Hdepleted. It is possible that changes in North Atlantic Ocean surface temperatures or changes in the position of the Gulf Stream could cause changes in the amount or isotopic composition of moisture sourced from this region to southern Baffin Island. However, sites influenced by the Gulf Stream exhibit stable sea surface temperatures during the past 6 ka (Solignac et al., 2004), suggesting that changes in North Atlantic-sourced moisture did not cause mean annual precipitation $\delta^2 H \mbox{ variability on southern Baffin}$ Island.

The QPT $C_{22}n$ -alkanoic acid δ^2H record exhibits some broad similarities with late summer temperature in the Labrador Sea (Gibb *et al.*, 2015; Fig. 5): both have high and stable values from 4.0 to 2.0 ka, with lower values before and after that. The $C_{22}n$ -alkanoic acid δ^2H record is correlated to Labrador Sea summer surface temperatures (p < 0.05 in 69.5% of ensemble runs), which we consider robust despite age model uncertainty. This correlation also makes physical sense: modern observations show that evaporation over Arctic seas in the late summer and early autumn dramatically increases

under warmer conditions (Boisvert and Stroeve, 2015). Thus, higher summer temperatures in the Labrador Sea would cause an increase in evaporation and delivery of moisture from this local source to southern Baffin Island. Increased local moisture delivery, primarily concentrated in late summer and autumn, would result in relatively ²H-enriched mean annual precipitation δ^2 H values at Lake QPT. We infer that warmer Labrador Sea surface conditions around 4.5-2.0 ka resulted in greater Labrador Sea evaporation and more ²H-enriched precipitation falling on southern Baffin Island, probably causing some of the variability that we observe in the Lake QPT leaf wax-inferred mean annual precipitation $\delta^2 H$ record. While sea ice retreat will probably contribute to large increases in locally evaporated autumn and winter Arctic precipitation in the next century (Bintanja and Selten, 2014; Singh et al., 2017), this record from southern Baffin Island suggests that changes in ocean temperature may exert a larger influence on evaporation in some high-latitude regions.

Climate at QPT in context with other Arctic regions

Lakes that reflect mean annual precipitation isotope values are useful to evaluate the regional influence of sea ice and other seasonal changes on precipitation in the Arctic. Although sea ice cover does not appear to be the main variable controlling the Lake QPT mean annual precipitation δ^2 H record, sea ice may be much more influential in coastal Greenland. Lake N3 in western Greenland, for example, has been interpreted to respond sensitively (>100% shifts in $C_{24}n$ -alkanoic acid δ^2H values) to changes in sea ice extent or other seasonal changes in lake ice cover and through-flow dynamics through the Holocene, owing partially to the study site's position north of the modern seasonal sea ice front (Thomas et al., 2016, 2020). Western Greenland may have experienced a large increase in winter precipitation amount or more ²H-depleted winter precipitation because of a stronger and warmer West Greenland Current and a corresponding decrease in sea ice in northern Baffin Bay (Thomas et al., 2016). Thus, although western Greenland and southern Baffin Island probably receive precipitation from similar moisture sources, it is possible that changes in ocean circulation and position of the study locations relative to the sea ice front affect precipitation isotopes in these two regions very differently.

The δ^2 H of aquatic plant-derived mid-chain *n*-alkanoic acids at lake Austre Nevlingen on northern Svalbard also reflects amountweighted mean annual precipitation δ^2 H (Kjellman et al., 2020). Reduced seasonal sea ice duration around Svalbard in the early Holocene is coincident with ²H-depleted mid-chain *n*-alkanoic acids, suggesting that, unlike southern Baffin Island, enhanced local winter moisture transport is strongly linked to reduced sea ice cover (Kjellman et al., 2020). The different mechanisms causing changes in mean annual precipitation δ^2H between these two regions could be due to differences in seasonal precipitation regimes on Baffin Island and on Svalbard. At present, Baffin Island has a seasonally variable precipitation amount, with dry winters and moist summers, while Svalbard experiences muted changes in seasonal precipitation amount, with winters slightly wetter than summers (Kjellman et al., 2020). In addition, northern Svalbard is close to the seasonal sea ice minimum extent, and therefore may be more strongly impacted by changes in sea ice than southern Baffin Island, which is close to the seasonal sea ice maximum (Fig. 1).

Many plant wax δ^2H records in the Arctic reveal changes in summer precipitation isotopes and aridity through time. A Holocene plant wax n-alkane δ^2H record from the Faroe Islands is interpreted to indicate that summers became progressively drier through the Holocene, as the fraction of poleward moisture transport declined with decreasing temperatures (Curtin

et al., 2019). On south-eastern Greenland, plant wax n-alkane δ^2 H is interpreted to show that Flower Valley Lake was evaporation-dominated through the mid-Holocene, before becoming precipitation-dominated around 4.1 ka as summers cooled (Balascio et al., 2013). Unlike Lake QPT, in both of these studies, mid- and long-chain plant waxes appear to reflect distinctly different plant sources, allowing a distinction between the isotopic composition of terrestrial and aquatic plant source water pools. These records provide insight into summer moisture source history, in contrast to Lake QPT, which reflects changes in mean annual precipitation. These different plant wax δ²H interpretations highlight the need to assess changes in seasonal precipitation dynamics throughout the Arctic, which can reveal how different regions are sensitive to different mechanisms of precipitation change. Mean annual precipitation isotopes and precipitation seasonality on southern Baffin Island seem to be most sensitive to changes in local sea surface temperature during the summer and autumn, whereas other regions are more sensitive to sea ice duration and/or changes in poleward moisture transport.

Conclusions

By comparing plant wax data (relative abundance and δ^2H) with an existing sedaDNA dataset, we aimed to better define the relationship between plant wax isotope records, the plant community and regional climate on Baffin Island, which is often not fully described in plant wax paleoclimate studies. While the vascular plant community at Lake QPT was relatively stable throughout the record, n-alkanoic acid distributions appear to reflect an increased contribution from aquatic mosses towards the present. Yet, this increase in aquatic moss n-alkanoic acids to the Lake QPT sediment does not appear to coincide with changes in the $C_{22}n$ -alkanoic acid δ^2H values, and thus changes in plant community do not appear to influence the δ^2H record. Instead, we interpret $C_{22}n$ -alkanoic acid δ^2H at Lake QPT to predominantly track changes in lake water δ^2H .

As modern QPT lake water reflects amount-weighted mean annual precipitation, we interpret mid-chain n-alkanoic acid $\delta^2 H$ in Lake QPT to reflect changes in mean annual precipitation $\delta^2 H$, inferred from mid-chain aquatic plant waxes, is not sensitive to changes in seasonal sea ice duration in the Labrador Sea, which is probably the dominant local moisture source to southern Baffin Island, but is significantly correlated to late summer temperatures in the Labrador Sea. We therefore infer that changes in summer and autumn evaporation from the Labrador Sea during the middle Holocene caused the changes in the QPT $C_{22}n$ -alkanoic acid $\delta^2 H$ record. When compared to other Holocene coastal precipitation isotope records in the Arctic, this study highlights regional differences in the Arctic hydrological cycle's response to changes in temperature and sea ice cover.

Acknowledgements. We thank the Qikiqtani Inuit and the Nunavut Research Institute for access to the field site (Nunavut Research Institute license no. 01 019-16N-A). This research was supported by the National Science Foundation (NSF ARCSS Grant No. 1737716 and EAR-IF Grant No. 1652274 to E.K.T.; NSF ARCSS Grant No. 1737712 to G.H.M. and J.S.; NSF GSS Grant No. 1657743 to G.H.M. and S.E.C.). We thank O. Cowling for laboratory assistance.

Conflict of interest—The authors report no conflicts of interest.

Data availability statement

The data that support the findings of this study will be made available via the National Centers for Environmental Information (NCEI) paleoclimate database maintained by the National Oceanic and Atmospheric Administration before publication, and we include a file of that same data along with this submission for use by the reviewers during the review process.

Supporting information

Additional supporting information can be found in the online version of this article.

Figure S1. Top: Bacon age model for Lake QPT sediment; blue and magenta symbols represent calibrated radiocarbon age distributions for samples collected from QPT16-3A and QPT16-2A, respectively; green point represents the inferred age of the core top. Bottom: magnetic susceptibility (MS) data for both cores. The gradational shaded area represents a decreasing contribution of clastic sediment towards the contact with gyttja in the Lake QPT record. Loop indicates values measured with a loop sensor on the whole core; high-resolution MS (HRMS) indicates values measured with a point sensor on the split core face.

Figure S2. Top: Downcore δ^2H of all n-alkanoic acid chain lengths (C_{20} – C_{30}). Bottom: dry weight concentration of all n-alkanoic acid chain lengths in downcore sediment. The gray shaded region indicates clastic sediment in the earliest part of the QPT record. The vertical black line indicates the timing of sedaDNA-inferred Betula sp. appearance in the Lake QPT catchment (Crump et al., 2019).

Supporting information.

Abbreviations. CI, confidence interval; DCM, dichloromethane; EA, elemental analyzer; FAME, fatty acid methyl esters; FID, flame ionization detector; GC, gas chromatograph; IRIS, isotope ratio infrared spectroscopy; IRMS, isotope ratio mass spectrometer; NCEI, National Centers for Environmental Information; SD, standard deviation; SEM, standard error of the mean; TOC, total organic carbon; VSMOW, Vienna Standard Mean Ocean Water.

References

- Anderson BT, Feldl N, Lintner BR. 2018. Emergent behavior of Arctic precipitation in response to enhanced Arctic warming. *Journal of Geophysical Research: Atmospheres* **123**: 2704–2717.
- Anderson RK, Miller GH, Briner JP *et al.* 2008. A millennial perspective on Arctic warming from ¹⁴C in quartz and plants emerging from beneath ice caps. *Geophysical Research Letters* **35**.
- Balascio NL, D'Andrea WJ, Bradley RS et al. 2013. Biogeochemical evidence for hydrologic changes during the Holocene in a lake sediment record from southeast Greenland. Holocene 23: 1428–1439.
- Bintanja R, Andry O. 2017. Towards a rain-dominated Arctic. *Nature Climate Change* **7**: 263–267. https://doi.org/10.1038/nclimate3240 Bintanja R, Selten FM. 2014. Future increases in Arctic precipitation
- linked to local evaporation and sea-ice retreat. *Nature* **509**: 479–482.
- Blaauw M, Christen JA. 2011. Flexible paleoclimate age-depth models using an autoregressive gamma process. *Bayesian Analysis* 3: 457–474.
- Blake W. 1991. Ratios of stable carbon isotopes in some High Arctic plants and lake sediments. *Journal of Paleolimnology* **6**: 157–166.
- Boisvert LN. 2015. The Arctic is becoming warmer and wetter as revealed by the Atmospheric Infrared Sounder. *Geophysical Research Letters* **42**: 4439–4446.
- Bowen GJ. 2017. The Online Isotopes in Precipitation Calculator, version 3.1. www.waterisotopes.org.
- Bowen GJ, Revenaugh J. 2003. Interpolating the isotopic composition of modern meteoric precipitation. *Water Resources Research* **39**.
- Briner JP, Davis PT, Miller GH. 2009. Latest Pleistocene and Holocene glaciation of Baffin Island, Arctic Canada: Key patterns and chronologies. *Quaternary Science Reviews* **28**: 2075–2087.
- Briner JP, McKay NP, Axford Y et al. 2016. Holocene climate change in Arctic Canada and Greenland. *Quaternary Science Reviews* 147: 340–364.

- Castañeda IS, Schouten S. 2011. A review of molecular organic proxies for examining modern and ancient lacustrine environments. *Quaternary Science Reviews* **30**: 2851–2891.
- Chikaraishi Y, Naraoka H. 2003. Compound-specific δD–δ13C analyses of n-alkanes extracted from terrestrial and aquatic plants. *Phytochemistry* **63**: 361–371.
- Cluett AA, Thomas EK, Evans SM *et al.* 2021. Seasonal variations in moisture origin explain spatial contrast in precipitation isotope seasonality on coastal western Greenland. *Journal of Geophysical Research, Atmospheres* **126**: e2020JD033543.
- Collins M, Knutti R, Arblaster J *et al.* 2013 Long-term climate change: projections, commitments and irreversibility. In Climate Change: The Physical Science Basis. Contribution of Working Group I to the Fifth Assessment Report of the Intergernmental Panel on Climate Change, Stocker TF, Qin D, Plattner G-K, Tignor M, Allen SK, Boschung J, Nauels A, Xia Y, Bex V, Midgley PM (eds). Cambridge University Press: Cambridge; 1029–1136.
- Crump SE, Miller GH, Power M *et al.* 2019. Arctic shrub colonization lagged peak postglacial warmth: molecular evidence in lake sediment from Arctic Canada. *Global Change Biology* **25**: 4244–4256.
- Curtin L, D'Andrea WJ, Balascio N et al. 2019. Holocene and Last Interglacial climate of the Faroe Islands from sedimentary plant wax hydrogen and carbon isotopes. *Quaternary Science Reviews* 223.
- Daniels WC, Russell JM, Giblin AE *et al.* 2017. Hydrogen isotope fractionation in leaf waxes in the Alaskan Arctic tundra. *Geochimica et Cosmochimica Acta* 213: 216–236.
- Dion-Kirschner H, McFarlin JM, Masterson AL et al. 2020. Modern constraints on the sources and climate signals recorded by sedimentary plant waxes in west Greenland. *Geochimica et Cosmochimica Acta* **286**: 336–354.
- Dufour A, Zolina O, Gulev SK. 2016. Atmospheric moisture transport to the Arctic: assessment of reanalyses and analysis of transport components. *Journal of Climate* 29: 5061–5081.
- Environment Canada. 2020. *Historical Climate Data*. Retrieved from https://climate.weather.gc.ca/index_e.html
- Fettweis X, Franco B, Tedesco M *et al.* 2013. Estimating the Greenland ice sheet surface mass balance contribution to future sea level rise using the regional atmospheric climate model MAR. *Cryosphere* **7**: 469–489.
- Florian CR, Miller GH, Fogel ML *et al.* 2015. Algal pigments in Arctic lake sediments record biogeochemical changes due to Holocene climate variability and anthropogenic global change. *Journal of Paleolimnology* **54**: 53–69.
- Freimuth EJ, Diefendorf AF, Lowell TV *et al.* 2019. Sedimentary nalkanes and n-alkanoic acids in a temperate bog are biased toward woody plants. *Organic Geochemistry* **128**: 94–107.
- Gao L, Edwards EJ, Zeng Y *et al.* 2014. Major evolutionary trends in hydrogen isotope fractionation of vascular plant leaf waxes. *PLoS ONE* **9**: e112610.
- Gao L, Hou J, Toney J *et al.* 2011. Mathematical modeling of the aquatic macrophyte inputs of mid-chain n-alkyl lipids to lake sediments: implications for interpreting compound specific hydrogen isotopic records. *Geochimica et Cosmochimica Acta* **75**: 3781–3791.
- Gibb OT, Steinhauer S, Fréchette B *et al.* 2015. Diachronous evolution of sea surface conditions in the Labrador Sea and Baffin Bay since the last deglaciation. *Holocene* **25**: 1882–1897.
- Hou J, D'Andrea WJ, MacDonald D *et al.* 2007. Hydrogen isotopic variability in leaf waxes among terrestrial and aquatic plants around Blood Pond, Massachusetts (USA). *Organic Geochemistry* **38**: 977–984.
- Hurrell JW, Deser C. 2010. North Atlantic climate variability: the role of the North Atlantic Oscillation. *Journal of Marine Systems* **79**: 231–244.
- IAEA/WMO. 2015. Global Network of Isotopes in PrecipitationThe GNIP Database. https://nucleus.iaea.org/wiser
- Jonsson CE, Leng MJ, Rosqvist GC *et al.* 2009. Stable oxygen and hydrogen isotopes in sub-arctic lake waters from northern Sweden. *Journal of Hydrology* **376**: 143–151.
- Kjellman SE, Schomacker A, Thomas EK et al. 2020. Holocene precipitation seasonality in northern Svalbard: influence of sea ice and regional ocean surface conditions. *Quaternary Science Reviews* **240**.
- Konecky BL, McKay NP, Churakova OV *et al.* 2020. The Iso2k database: a global compilation of paleo-δ18O and δ2H records to aid understanding of Common Era climate. *Earth System Science Data* **12**: 2261–2288

- Lamhonwah D, Lafrenière MJ, Lamoureux SF *et al.* 2017. Evaluating the hydrological and hydrochemical responses of a High Arctic catchment during an exceptionally warm summer. *Hydrological Processes* **31**: 2296–2313.
- Lecavalier BS, Fisher DA, Milne GA et al. 2017. High Arctic Holocene temperature record from the Agassiz ice cap and Greenland ice sheet evolution. Proceedings of the National Academy of Sciences of the United States of America. 114: 5952–5957
- Lee H, Feakins SJ, Lu Z et al. 2017. Comparison of three methods for the methylation of aliphatic and aromatic compounds. Rapid Communications in Mass Spectrometry 31: 1633–1640.
- Longo WM, Dillon JT, Tarozo R *et al.* 2013. Unprecedented separation of long chain alkenones from gas chromatography with a poly(trifluoropropylmethylsiloxane) stationary phase. *Organic Geochemistry* **65**: 94–102.
- Loranty MM, Goetz SJ, Beck PSA. 2011. Tundra vegetation effects on pan-Arctic albedo. *Environmental Research Letters* **6**.
- McFarlin JM, Axford Y, Masterson AL *et al.* 2019. Calibration of modern sedimentary δ^2 H plant wax-water relationships in Greenland lakes. *Quaternary Science Reviews* **225**.
- McKay NP, Emile-Geay J, Khider D. 2020. GeoChronR an R package to model, analyze and visualize age-uncertain paleoscientific data. *Geochronology Discussions* **2020**: 1–33.
- Miller GH. 1980. Late Foxe glaciation of southern Baffin Island, N.W.T., Canada. Geological Society of America Bulletin 91: 399–405.
- Miller GH, Alley RB, Brigham-Grette J et al. 2010. Arctic amplification: can the past constrain the future? *Quaternary Science Reviews* **29**: 1779–1790.
- Miller GH, Lehman SJ, Refsnider KA *et al.* 2013. Unprecedented recent summer warmth in Arctic Canada. *Geophysical Research Letters* **40**: 5745–5751.
- National Snow and Ice Data Center. 2018. SOTC: Sea ice. Retrieved from nsidc.org/cryosphere/sotc/sea_ice.html
- Nesje A. 1992. A piston corer for lacustrine and marine sediments. *Arctic and Alpine Research* **24**: 257–259.
- Nusbaumer J, Alexander PM, LeGrande AN et al. 2019. Spatial shift of Greenland moisture sources related to enhanced Arctic warming. Geophysical Research Letters 46: 14723–14731.
- O'Connor KF, Berke MA, Ziolkowski LA. 2020. Hydrogen isotope fractionation in modern plants along a boreal-tundra transect in Alaska. *Organic Geochemistry* **147**.
- Osburn CL, Anderson NJ, Leng MJ *et al.* 2019. Stable isotopes reveal independent carbon pools across an Arctic hydro-climatic gradient: implications for the fate of carbon in warmer and drier conditions. *Limnology and Oceanography Letters* **4**: 205–213.
- Overland JE, Wang M, Walsh JE *et al.* 2014. Future Arctic climate changes: adaptation and mitigation time scales. *Earth's Future* 2: 68–74.
- Pendleton SL, Miller GH, Anderson RA *et al.* 2017. Episodic neoglacial expansion and rapid 20th century retreat of a small ice cap on Baffin Island, Arctic Canada, and modeled temperature change. *Climate of the Past* **13**: 1527–1537.
- Putman AL, Feng X, Sonder LJ *et al.* 2017. Annual variation in event-scale precipitation $\delta^2 H$ at Barrow, AK, reflects vapor source region. *Atmospheric Chemistry and Physics* **17**: 4627–4639.
- Rach O, Kahmen A, Brauer A et al. 2017. A dual-biomarker approach for quantification of changes in relative humidity from sedimentary lipid D/H ratios. Climate of the Past 13: 741–757.

- Reimer PJ, Bard E, Bayliss A *et al.* 2013. Selection and treatment of data for radiocarbon calibration: an update to the international calibration (IntCal) criteria. *Radiocarbon* **55**: 1923–1945.
- Sachse D, Billault I, Bowen GJ et al. 2012. Molecular paleohydrology: interpreting the hydrogen-isotopic composition of lipid biomarkers from photosynthesizing organisms. *Annual Review of Earth and Planetary Sciences* **40**: 221–249.
- Sauer PE. 1997. Record of climate and late quaternary paleoclimate from stable isotopes in lakes and lake sediments, eastern Canadian Arctic. [Doctoral dissertation]. University of Colorado Boulder.
- Shuman B, Huang Y, Newby P *et al.* 2006. Compound-specific isotopic analyses track changes in seasonal precipitation regimes in the Northeastern United States at ca 8200calyrBP. *Quaternary Science Reviews* **25**: 2992–3002.
- Singh HKA, Bitz CM, Donohoe A *et al.* 2017. A source–receptor perspective on the polar hydrologic cycle: sources, seasonality, and Arctic–Antarctic parity in the hydrologic cycle response to CO₂ doubling. *Journal of Climate* **30**: 9999–10017.
- Sodemann H, Schwierz C, Wernli H. 2008. Interannual variability of Greenland winter precipitation sources: Lagrangian moisture diagnostic and North Atlantic Oscillation influence. *Journal of Geophysical Research* 113: D3.
- Solignac S, de Vernal A, Hillaire-Marcel C. 2004. Holocene seasurface conditions in the North Atlantic contrasted trends and regimes in the western and eastern sectors (Labrador Sea vs. Iceland Basin). *Quaternary Science Reviews* **23**: 319–334.
- Stevenson MA, McGowan S, Pearson EJ et al. 2020. Characterising organic carbon sources in Anthropocene affected Arctic upland lake catchments, Disko Island, West Greenland. *Biogeosciences Discussions* **2020**: 1–32.
- Sturm M, Douglas T, Racine C et al. 2005. Changing snow and shrub conditions affect albedo with global implications. *Journal of Geophysical Research* **110**: G1.
- Swann AL, Fung IY, Levis S et al. 2010. Changes in Arctic vegetation amplify high-latitude warming through the greenhouse effect. *Proceedings of the National Academy of Sciences of the United States of America* **107**: 1295–1300.
- Taberlet P, Coissac E, Pompanon F *et al.* 2007. Power and limitations of the chloroplast trn L (UAA) intron for plant DNA bar coding. *Nucleic Acids Research* **35**: e14–e14.
- Thomas EK, Briner JP, Ryan-Henry JJ *et al.* 2016. A major increase in winter snowfall during the Middle Holocene on western Greenland caused by reduced sea ice in Baffin Bay and the Labrador Sea. *Geophysical Research Letters* **43**: 5302–5308.
- Thomas EK, Hollister KV, Cluett AA *et al.* 2020. Reconstructing Arctic precipitation seasonality using aquatic leaf wax δ^2H in lakes with contrasting residence times. *Paleoceanography and Paleoclimatology* **35**: e2020.
- van den Broeke M, Bamber J, Ettema J *et al.* 2009. Partitioning recent Greenland mass loss. *Science* **326**: 984–986.
- van Geldern R, Barth JAC. 2012. Optimization of instrument setup and post-run corrections for oxygen and hydrogen stable isotope measurements of water by isotope ratio infrared spectroscopy (IRIS). *Limnology and Oceanography: Methods* **10**: 1024–1036.
- Wolfe AP. 2003. Diatom community responses to late-Holocene climatic variability, Baffin Island, Canada: a comparison of numerical approaches. *Holocene* **13**: 29–37.